Research Article

Journal of Environmental Nanotechnology

Microstructural, Mechanical, and Thermal Characterization of TiO_2- and ZrO_2-reinforced Aluminum Matrix Nanocomposites Fabricated Using Powder Metallurgy

T. Shaafi[1], M. Kalaimani[1*], M. Yuvaperiyasamy[1], V. Jeyabalaji[2] and Krishna Prakash Arunachalam[3]

[1]Department of Mechanical Engineering, Saveetha School of Engineering, Saveetha Institute of Medical and Technical Sciences (SIMATS), Chennai, TN, India

[2]Department of Mechanical Engineering, SRM Madurai College for Engineering and Technology, Sivagangai, TN, India

[3]Departamento de Ciencias de la Construcción, Facultad de Ciencias de la Construcción Ordenamiento Territorial, Universidad Tecnológica Metropolitana, Santiago, Chile

Received: 22.05.2025 Accepted: 18.06.2025 Published: 30.06.2025

*mkalaikvn@gmail.com

ABSTRACT

This study investigates the development and characterization of aluminum-based nanocomposites reinforced with varying amounts of 0, 3, 6, and 9 weight percentages of titanium dioxide (TiO_2) and zirconium dioxide (ZrO_2) nanoparticles. The nanocomposites, designated as Al/TiO_2 and Al/ZrO_2, were fabricated by powder metallurgy processes and sintered at 550 °C using a tubular furnace. The comprehensive test was conducted using scanning electron microscopy (SEM), Energy dispersive x-ray spectroscopy (EDX), density, and microhardness testing, as well as thermal conductivity analysis. EDX analysis revealed that the addition of TiO_2 and ZrO_2 reinforcements resulted in a proportional enhancement of the Ti and Zr peaks. The density measurements of the materials indicated that adding reinforcements increased porosity to 2.85% for Al-9% TiO_2 and 5.26% for Al-9% ZrO_2. The microhardness values attained were 70.70 HV for Al-9% TiO_2 and 69.68 HV for Al-9% ZrO_2, indicating enhanced dispersion strengthening. In thermal conductivity analysis, the Al-9% TiO_2 and Al-9% ZrO_2 specimens exhibited low thermal conductivity values of 2.1 W/m·K and 2.06 W/m·K, respectively, at 300 °C, due to increased phonon scattering at the reinforcement-matrix interfaces. This thermal reduction was attributed to phonon scattering at the matrix reinforcement interfaces. The findings indicate that enhancing the nanocomposite strength results in a reduction of thermal conductivity. Results suggest that Al/TiO_2 and Al/ZrO_2 nanocomposites exhibit beneficial characteristics for applications demanding high strength, wear resistance, and thermal management.

Keyword: Titanium oxide; Zirconium oxide; Microhardness; Thermal conductivity.

1. INTRODUCTION

Researchers worldwide have turned their focus from monolithic to composite materials in response to the ever-increasing need for high-performance and cost-effective materials. An enormous amount of work has been done recently to create a variety of metal matrix composite combinations. Aluminum-based Metal Matrix Composites (MMCs) are considered superior structural materials due to their high specific modulus, low weight, excellent corrosion resistance, and wear resistance, making them ideal for automotive and aerospace applications (Samal *et al.* 2020). Composite materials are defined by material scientists as substances created through the mechanical interaction of more than two existing compounds, producing a whole new substance with characteristics that are different from those of its original components. The MMC functions as a reinforcing material, often composed of ceramic compounds, while enhancing physical properties including electrical and thermal conductivity, modulus of elasticity, resistance to wear and corrosion, and strength. The most commonly used ceramic particles are silicon carbide (SiC), boron carbide (B_4C), titanium carbide (TiC), aluminum oxide (Al_2O_3), zirconium carbide (ZrC), titanium dioxide (TiO_2), and zirconium dioxide (ZrO_2). ZrO_2 and TiO_2 are the most effective ceramic reinforcement particulates in terms of thermal stability aspects. Song *et al.* (2023) found that Zirconia (ZrO_2) displays superior ionic conductivity, corrosion resistance, fracture toughness, and mechanical strength. It is extensively utilized in applications such as thermal coatings for barriers, indicators, and thermal resistive material. The improved performance of aluminum strengthened with nano-ceramic particles is based on fundamental physical principles. Due to their high surface area-to-volume ratio, nanoparticles enhance stress transmission under mechanical loads by generating better interfacial interaction with the aluminum matrix. Their tiny size also leads to efficient grain refinement

through grain boundary pinning (Zener pinning), which restricts grain growth and enhances strength according to the Hall–Petch relationship. Furthermore, the consistent distribution of nanoparticles hinders dislocation movement more than microparticles, hence improving hardness and wear resistance by means of Orowan strengthening and load sharing (Surakasi *et al.* 2022).

Aluminum nanocomposites were made by stir casting aluminum alloys with various weight percentages of nano-sized zirconium oxide (ZrO_2) in a controlled atmosphere. The addition of ZrO_2 nanoparticles to an aluminum nanocomposite enhanced its tribological properties by increasing the coefficient of friction and wear resistance associated with the base matrix. This, in turn, improved the material's mechanical properties, including its ultimate tensile strength, impact strength, and microhardness (Kumar and Irfan, 2021).

Aluminum nanocomposites were fabricated through rolling, incorporating varying weight percentages of nano-sized titanium oxide (TiO_2). The tribological behaviour of aluminum nanocomposites improved with an increase in the coefficient of friction and wear resistance, which are associated with the base matrix and enhanced mechanical properties, due to the cumulative volume percentage of TiO_2 nanoparticles (Najjar *et al.* 2023).

Many researchers are focusing on the development of aluminum nanocomposites, considering various environmental aspects, including heat, chemical, and corrosion resistance (Randis *et al.* 2023). Stir casting was used to investigate the physical and corrosion behaviour of Al-2024 alloy strengthened with 0–6 wt.% ZrO_2 nanoparticles. With rising ZrO_2 concentration, hardness improved; in a 3.5% NaCl solution, corrosion resistance rose appreciably (Kennedy *et al.* 2021). The mechanical properties of monolithic and nanocomposites reinforced with 0–3 wt.% TiO_2 nanoparticles were monitored over several ARB (Accumulative Roll Bonding) passes. The microstructure of the composite reveals that after five rolling passes, the reinforcement particles, ultrafine grains, and elongated matrix grains are uniformly distributed. The TiO_2 particles were uniformly spread after five ARB passes, and Vickers microhardness grows with roll bonding passes (Najjar and Elmahdy, 2022). Thermal conductivity is the most important thermal property for aluminum nanocomposites, as they must retain structural stability and resist dimensional changes and material expansion (Zhang and Li, 2023).

The maximum heat flux for Al_2O_3 material is measured at 16,000 W/m². In contrast, TiO_2 coatings exhibit a heat flux dissipation of 15,000 W/m², while ZrO_2 coatings show a convective heat flux dissipation of 14,000 W/m². Uncoated materials demonstrate a total heat flux in the range of 8,036 W/m² (Sunil *et al.* 2023). TiO_2-ZrO_2 films exhibit higher hardness values than TiO_2 thin films. The presence of ZrO_2 in TiO_2-ZrO_2 thin films inhibits the crystallization of TiO_2 post-annealing, in contrast to TiO_2 thin films, leading to improved surface quality and enhanced thermal stability after the annealing process (Sezgin *et al.* 2023). Al/TiO_2–ZrO_2 coating at a nanoparticle concentration of 3 wt%. Nonetheless, a decline in mechanical properties was observed beyond 3 wt.%, attributed to the accumulation of nano-TiO_2–ZrO_2 particles within the PU (polyurethane) matrix. The PU–AT/TiO_2–ZrO_2 formulation demonstrates superior hydrophobic properties, as indicated by a water contact angle of 116.9º. In conclusion, the investigations indicated that the newly combined PU–AT/TiO_2–ZrO_2 nanocomposite exhibited superior barrier, mechanical, and hydrophobic properties. The incorporation of AT/TiO_2–ZrO_2 nanoparticles into the polyurethane effectively mitigated material degradation and contributed to the extended duration of the coated steel (Xavier, 2022). The Powder Metallurgy (PM) fabrication method provides a more versatile and adaptable approach for the mass production of components than traditional methods like casting precision components (Manohar *et al.* 2021). The integration of optimized manufacturing techniques with novel material systems facilitates the fabrication of this material. Powder metallurgy enhances material use efficiency by leveraging high density and superior mechanical properties (Boehlert *et al.* 2021). It minimizes machining requirements, simplifies complex shapes, enables the configuration of diverse variables, accommodates a broad spectrum of property variations, reduces potential waste and ensures a rapid production rate. The primary methods of powder manufacturing include mechanical, chemical, and physical techniques. Powder manufacture, mixing, compaction, and sintering are the four main components of the powder metallurgy process. A room-temperature compression phase is followed by an air pressure, high-temperature sintering phase. Powder metallurgy improves mechanical qualities, including hardness, tensile strength, compressive strength, and wear rate by reinforcing diverse materials with aluminum metal matrix composites (Singh *et al.* 2021).

The manufacturing method of aluminum composites through powder metallurgy with a muffle furnace provides multiple benefits that exceed other sintering processes. Through this technique, scientists have complete control over composition together with microstructure, which results in uniform distribution of reinforcement particles that improves mechanical properties (Madhusudhana *et al.* 2022; Nayak *et al.* 2022). A muffle furnace system controls the atmosphere to decrease oxidation, leading to better total sintering results. Sintering occurs at reduced energy consumption through shorter durations and lower temperatures because of this method. The muffle furnace sintering method represents a cost-effective alternative to hot

pressing and spark plasma sintering, which enables its use for industrial applications at scale (Arif *et al.* 2017). The production method generates composite materials that display enhanced hardness in addition to better tensile strength and wear resistance through an effective aluminum matrix-reinforcement bond. External pressure applied during sintering produces detrimental effects on particle morphology so its avoidance leads to preservation. The muffle furnace process of slow heating and cooling produces tighter material density and creates minimal residual stress buildup. Through this method, one can sinter complex-shaped parts without compromising quality (Panwar *et al.* 2020). Powder metallurgy production methods generate net-shaped products while minimizing material waste. The controlled muffle furnace environment protects the sample from contamination and produces high-purity end products (Kishore *et al.* 2023). The combined sintering process delivers aluminum composites suitable for aerospace applications, as well as automotive and structural purposes, due to its ability to maintain high quality and desired mechanical properties.

This study aims to develop Al/TiO_2 and Al/ZrO_2 nanocomposites using the powder metallurgy technique and assess their thermal conductivity behavior and physical characteristics. By including various weight percentages of TiO_2 and ZrO_2 nanoparticles, which are recognized for their exceptional abrasion resistance and thermal stability, the research emphasizes the heat resistance performance of these nanocomposites. This work addresses the research gap in the comprehensive investigation of the thermal conductivity of Al/TiO_2 and Al/ZrO_2 nanocomposites. Sintered in a muffle furnace at 550 °C, the nanocomposites underwent a comparative study to grasp the impact of each reinforcement. Though it improved porosity, ZrO_2 was shown to provide greater hardness, which compromised thermal performance. The research finds 9 wt.% nano-reinforcement as the best, since it provides a good mix of mechanical strength and low nanoparticle aggregation in both cases. In addition, as a result of this research, nanocomposites of Al/TiO_2 and Al/ZrO_2 that are suited for thermal applications have been developed.

2. MATERIALS AND METHODS

Aluminum powder with a purity of 99.0% and a density of 2.7 g/cm^3, with an average particle size is 20 to 50 µm, was chosen as the base powder for this study. Ceramic nano-reinforcement particles of TiO_2, with a purity of 99.0%, density of 4.23 g/cm^3, and particle size ranging from 20 to 40 nm, as well as ZrO_2 nano-reinforcement particles, with a purity of 99.0%, density of 5.68 g/cm^3, and particle size of 20 to 40 nm, as shown in Fig. 1, were obtained from Vedayukt India Pvt. Ltd., Jamshedpur, Jharkhand, India.

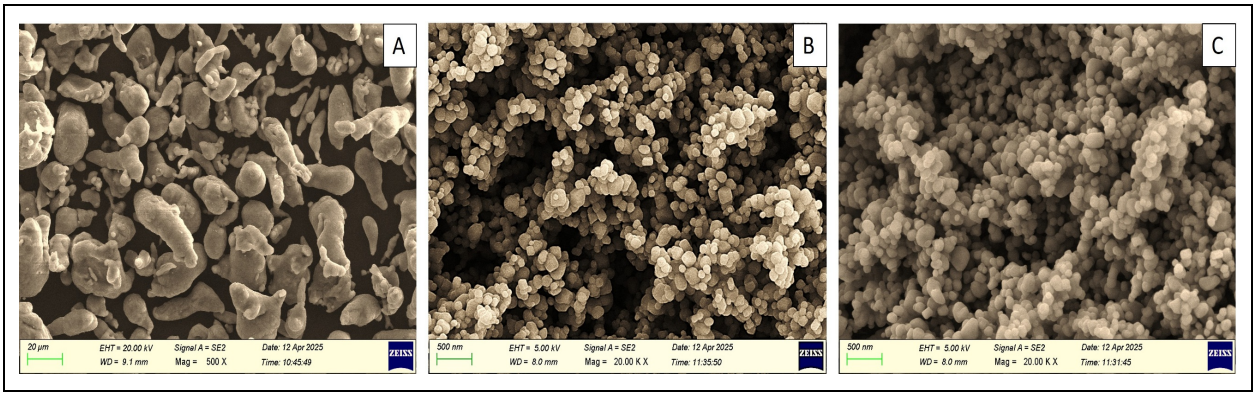


Fig. 1: (A) Aluminum particles, (B) Titanium dioxide, (C) Zirconium dioxide

Table 1. Sample compositions

Sample	Al (%)	TiO_2 (%)	ZrO_2 (%)
$A1_0$	100	-	-
AT_3	97	3	-
AT_6	94	6	-
AT_9	91	9	-
AZ_3	97	-	3
AZ_6	94	-	6
AZ_9	91	-	9

The nanocomposite powders were mixed as shown in Table 1, and each sample was processed using a high-energy ball mill for 5 hours in a VB Ceramic Planetary ball mill. The drum operated at a speed of 300 rpm. The tool used was a steel ball that was 10 mm in diameter, with a 5:1 ball-to-powder ratio. To keep the temperature from rising, a cooling procedure was used every 10 minutes (Khan *et al.* 2020). The green compacts were formed into billets, 8 mm in diameter and 30 mm in height, using a load cell hydraulic press at a pressure up to 600 MPa. Zinc stearate was employed as a lubricant to mitigate friction between the punch and die. Following that, the green compact samples were sintered at 550 °C

for 150 minutes in an electric tubular furnace under a controlled atmosphere to prevent oxidation as shown in Fig 2. The sintered samples were left in the furnace until they reached room temperature.

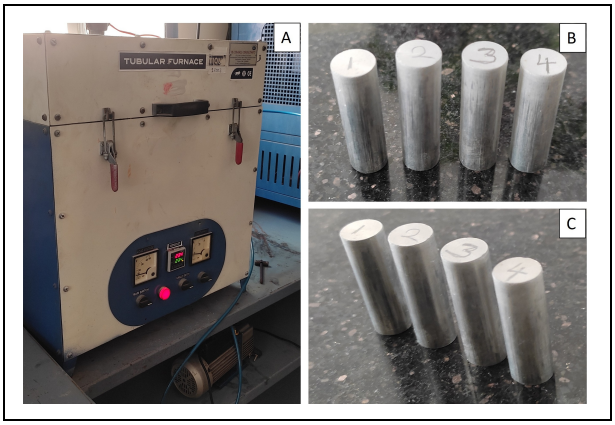


Fig. 2: Synthesis of composites: (A) Tubular furnace, (B) Al/TiO_2 nanocomposite, and (C) Al/ZrO_2 nanocomposite

The optimal standards for metallographic preparation must be ensured prior to the initiation of microstructural investigation. The Keller reagent was used for etching, which included 95 ml of distilled water, 2.5 ml of HNO_3, 1.5 ml of HCl, and 1.0 ml of HF. The surface morphology of the composites was analyzed using a ZEISS optical microscope. An X-ray diffraction analysis was conducted on the aluminum composites of samples utilizing the PANalytical X-Pert Pro MRD. The microstructural features were analyzed utilizing a Scanning electron microscope (JEOL 7900F) equipped with Energy dispersive x-ray spectroscopy (EDX).

The Archimedes principle can be used to quantitatively determine a nanocomposite's experimental density (ρ_{Exp}) using electronic weighing equipment with a density calculation function by Eq. (1) and following the ASTM D792-66 test procedure. (Juliyana *et al.* 2022).

$$Experimental\ density\ (\rho_{Exp}) = \frac{mass\ (g)}{volume\ (cm^3)} \quad \ldots (1)$$

The theoretical density (ρ_{Th}) of aluminum nanocomposite is determined by using the mass fraction of pure aluminum (m_{Al}), mass of nano-reinforcement particle (m_{Re}) ($m_{TiO_2}$and m_{ZrO_2}), in Eq. 2. The densities of aluminum, Titanium dioxide nanoparticles, and zirconium dioxide nanoparticles are ρ_{Al} = 2.7 g/cm³, ρ_{TiO_2} = 4.23 g/cm³, and ρ_{ZrO_2} = 5.68 g/cm³, respectively.

$$Theoritical\ density\ (\rho_{Th}) = (m_{Al}) \times (\rho_{Al}) + (m_{Re}) \times (\rho_{Re}) \quad \ldots (2)$$

The ratio of the experimental and theoretical density is the percentage of porosity, expressed by Eq. 3.

$$Porosity\ (\%) = \left(1 - \frac{\rho_{Exp}}{\rho_{Th}}\right) \times 100 \quad \ldots (3)$$

The microhardness strength quantifies the hardness of nanocomposite samples utilizing a Shimadzu HMV-2 Vickers hardness testing machine, following ASTM E384, conducted at room temperature. The yield strength test was performed on aluminum nanocomposite samples using a Universal testing machine (UTM) supported by the computerized servo-hydraulic system following the ASTM E-8-04 standard. According to the ASTM E9-09 standard, the aluminum nanocomposite was put through tensile test samples at room temperature (30 °C) using a computerized servo-hydraulic UTM. The Netzsch LFA 427 uses laser flash methodology. The samples are 10 mm in diameter and 3 mm in thickness. The surfaces are cleaned by immersing them in ethanol and ultrasonicated for 10 minutes, rinsed with deionized water to remove the solvent residues, and dried in compressed air. The thermal diffusivity and thermal conductivity were calculated by Eq. 4 and Eq. 5.

$$Thermal\ diffusivity\ (\alpha) = \frac{0.1388 \cdot L^2}{t_{1/2}} \quad \ldots (4)$$

The thermal diffusivity (mm^2/s) is calculated by L = sample thickness (m), $t_{1/2}$ = time taken at which the rear surface temperature reaches half its maximum value (s).

$$Thermal\ conductivity\ (k) = \propto \alpha.\rho.C_p \quad \ldots (5)$$

The thermal conductivity (W/m·K), is calculated by α = thermal diffusivity (mm^2/s) measured by experiment, ρ = density (kg/m^3) measured by Archimedes principle, C_p = specific heat capacity (J/kg·K) calculated from the oxide particles.

3. RESULTS AND DISCUSSION

3.1 Microstructure Analysis

The SEM micrographs shown in Fig. 3 reveal the surface morphology of aluminum nanocomposites with different TiO_2 reinforcement levels: ($A1_0$) pure aluminum, (AT_3) Al–3% TiO_2, (AT_6) Al–6% TiO_2, and (AT_9) Al–9% TiO_2, all at 50x. The unreinforced sample ($A1_0$) has a smooth surface with minimal particles, typical of pure aluminum. The AT_3 has noticeable TiO_2 particles evenly distributed in the matrix, good bonding, and minimal agglomeration at a lower reinforcement level (Sabari *et al.* 2025). The AT_9 sample has a more heterogeneous distribution. Clustering and agglomeration are more visible, which can be stress concentration points under mechanical loading. Despite the higher dispersion, some areas show microstructural inhomogeneity that can reduce ductility. In general, the micrographs show that high TiO_2 content makes the reinforcement spread out more; nevertheless, at high wt.% of TiO_2, it clumps together. Overweight of the nano-reinforcement particles may reduce their malleability and increase their structural stability

characteristics. This is in line with previous studies where the optimal amount of reinforcement improved mechanical properties, tribological and thermal resistance (Joshua *et al.* 2018). The SEM analysis confirms the effect of TiO_2 content on microstructural evolution and provides critical information for optimization of nanocomposite formulation for advanced engineering applications. TiO_2 particles act as nucleation sites, which makes the aluminum grains smaller and tougher, which contributes to their extended durability.

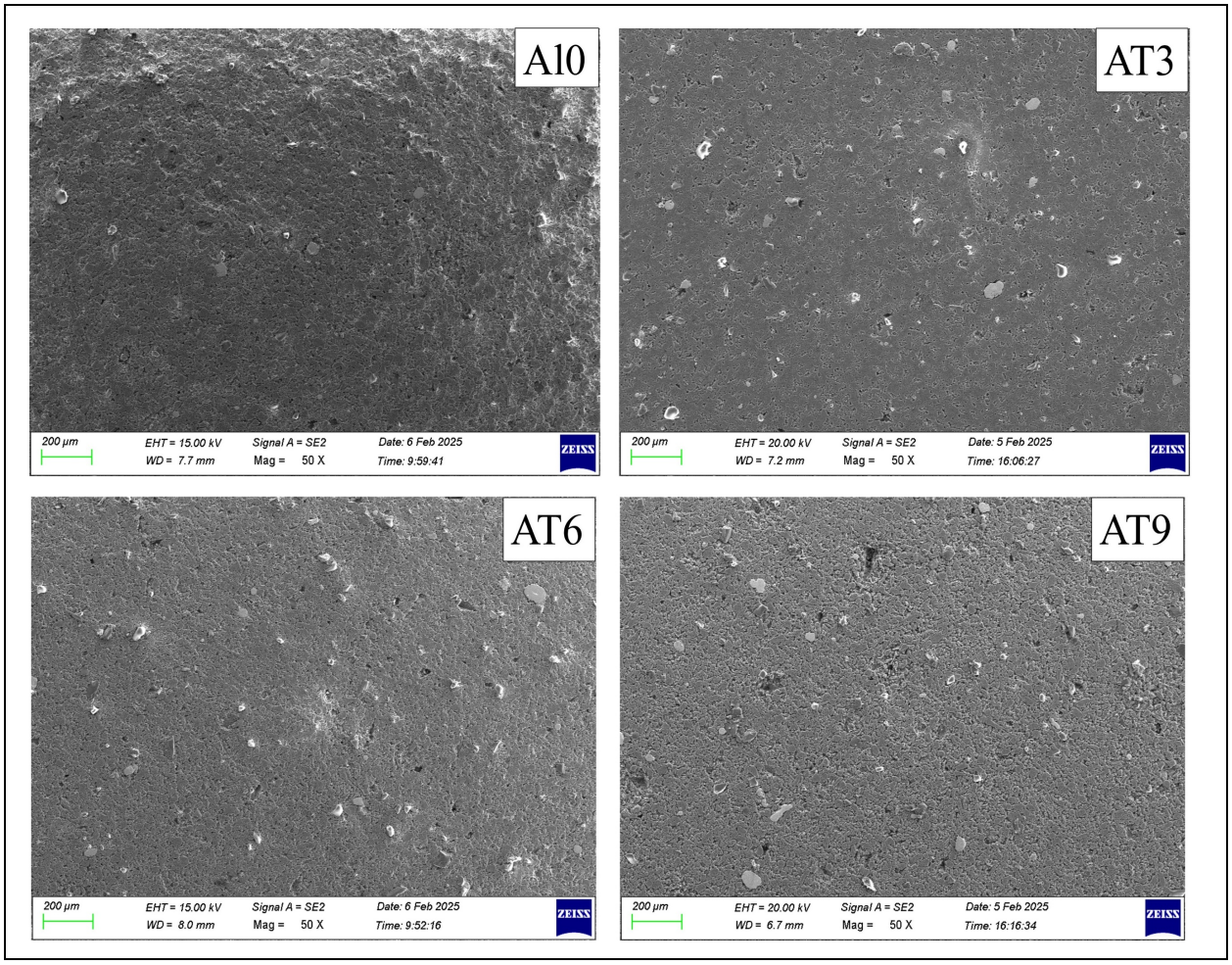


Fig. 3: SEM images of Aluminum nanocomposite samples: (Al_0) pure Al, (AT_3) Al-3% TiO_2, (AT_6) Al-6% TiO_2, and (AT_9) Al-9% TiO_2

The Al/ZrO_2 SEM analysis represented in Fig. 4 shows the microstructural evaluation of aluminum nanocomposites reinforced with a varying wt.% of ZrO_2. The sample $A1_0$ exhibits a smooth and relatively featureless surface morphology, characteristic of a metallic matrix with excellent particle interaction. The inclusion of the 3 wt.% ZrO_2 nano-reinforcement resulted in noticeable changes in the surface morphology as compared to the samples Al_0, highlighting the presence of well-dispersed nanoceramic particles throughout the matrix. These dispersed nano-reinforcements contribute to the grain boundary and serve as effective particle binding strength, enhancing the structural integrity of the composite. For further addition of reinforcement at 6 wt.%, the distribution of ZrO_2 seems denser, but does not remain homogenous, indicating strengthened nanocomposite interaction without significant particle clustering. This typical particle dispersion results in improved mechanical properties due to efficient load-bearing capacity and grain structural refinement (Luqman *et al.* 2023). However, increasing the concentration of nano-reinforcement at wt. 9% in the sample AZ_9 showed noteworthy agglomeration and clustering of ZrO_2 nanoparticles, which undermines microstructural homogeneity. The rougher surface contains a high concentration of ZrO_2 particles dispersed throughout the matrix. These particles appear brighter in the image due to the higher atomic number of zirconium. However, some particle agglomeration is visible, which could lead to localized stress points and affect the mechanical properties of the composite.

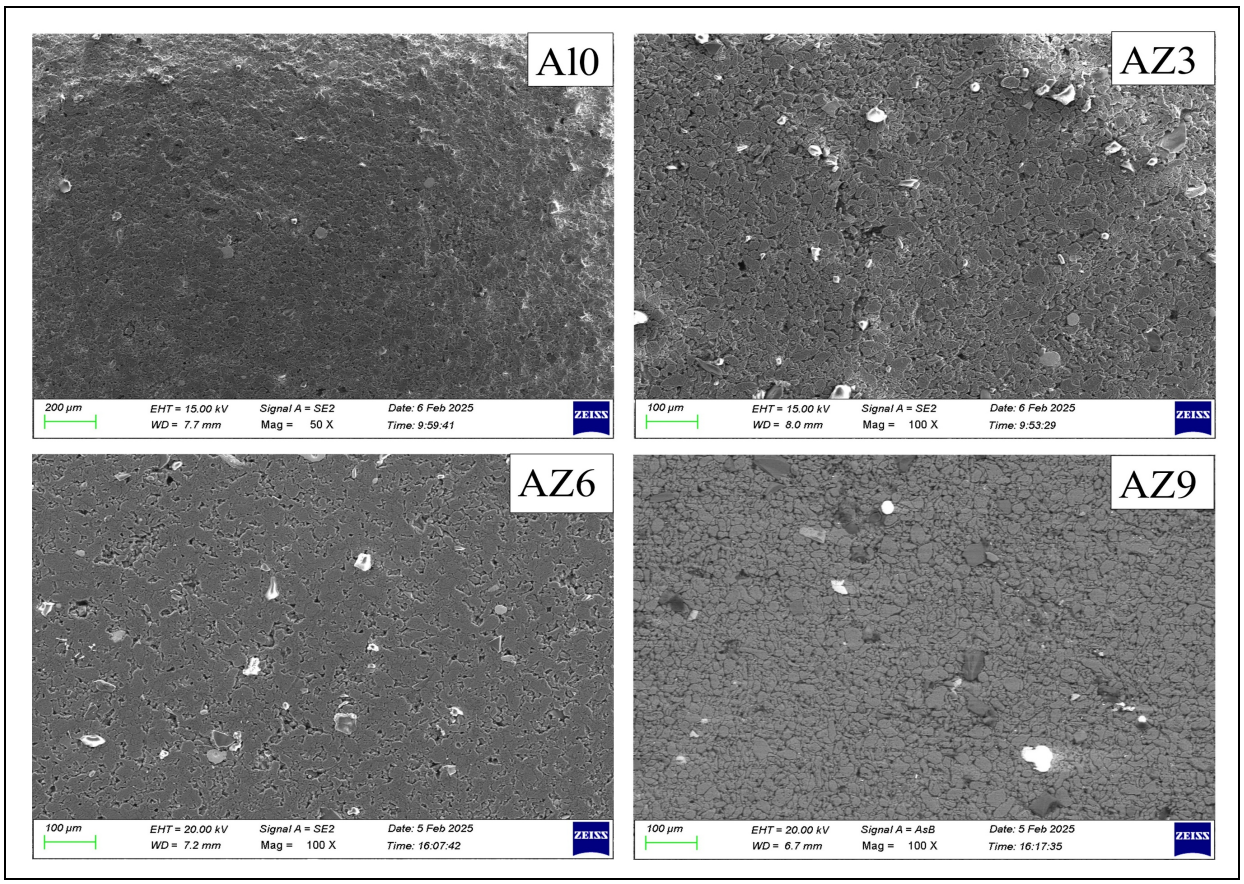


Fig. 4: SEM images of Aluminum nanocomposite samples: ($A1_0$) pure Al, (AZ_3) Al-3% ZrO_2, (AZ_6) Al-6% ZrO_2, and (AZ_9) Al-9% ZrO_2

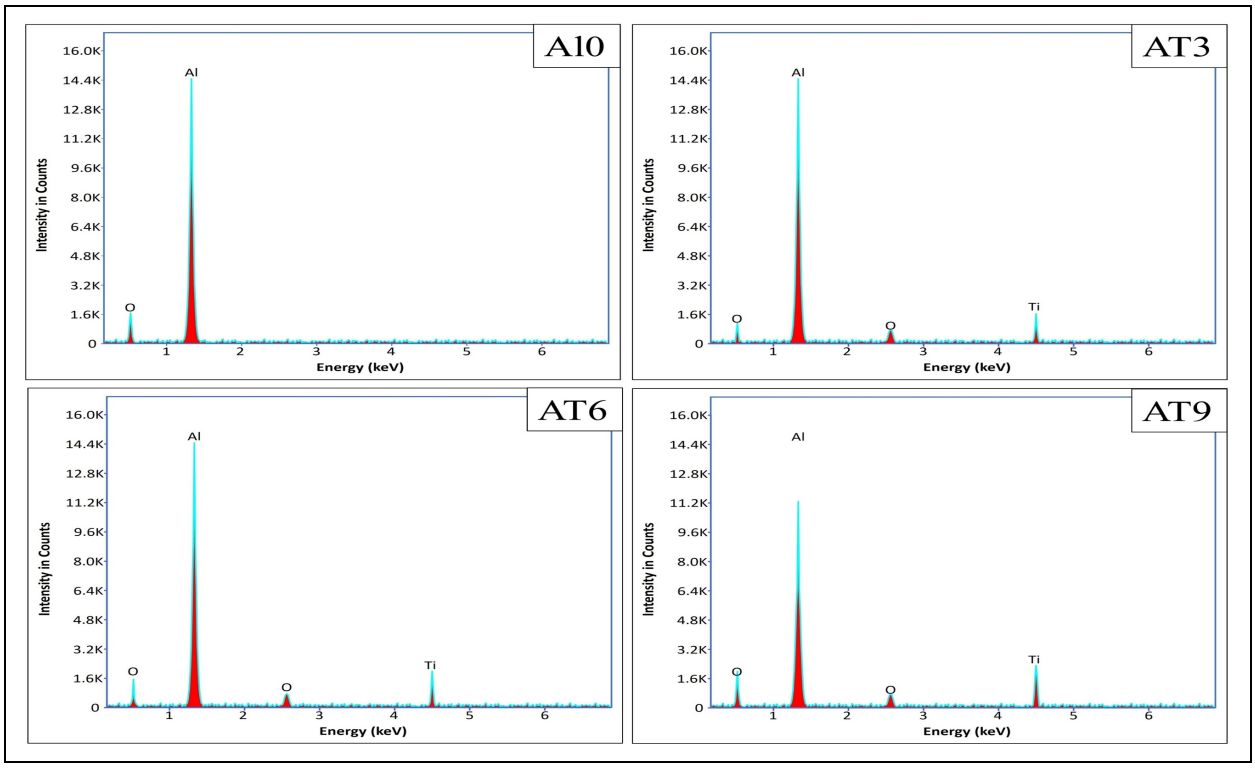


Fig. 5: EDX images for Al/TiO_2 composites

3.2 EDX Analysis

The EDX spectroscopy (Fig. 5) shows the material composition of pure aluminum ($A1_0$) in addition to aluminum matrix composites with TiO_2 concentrations of 3% (AT_3), 6% (AT_6), and 9% (AT_9). A dominant peak belonging to aluminum at 1.49 keV and a weak oxygen peak at ~0.52 keV emerge when studying the EDX spectrum of pure aluminum ($A1_0$). Surface oxidation is represented by this oxygen peak. An increase in TiO_2 nano-concentration leads to stronger peaks for oxygen and titanium elements in the EDX spectra of AT_3, AT_6, and AT_9. The Ti peaks located between 4.5 and 4.9 keV show that titanium from TiO_2 nanoparticles exists in the material, and they increase in prominence through AT_6 and AT_9. More oxide phase appears in the matrix as the intensification of oxygen peaks coincides with increasing TiO_2 content. The Al peak experiences gradual attenuation through all samples because the reinforcement introduces dilution effects. The stable elements detected in the analysis prove that TiO_2 particles maintain an even distribution inside the aluminum metal. The results showed no additional elemental peaks apart from the expected ones, thus indicating sample purity. The fabricated Al-TiO_2 composites underwent successful production according to these findings. The EDX results show both correct TiO_2 increase and intact bonding connections between reinforcing particles and matrix components.

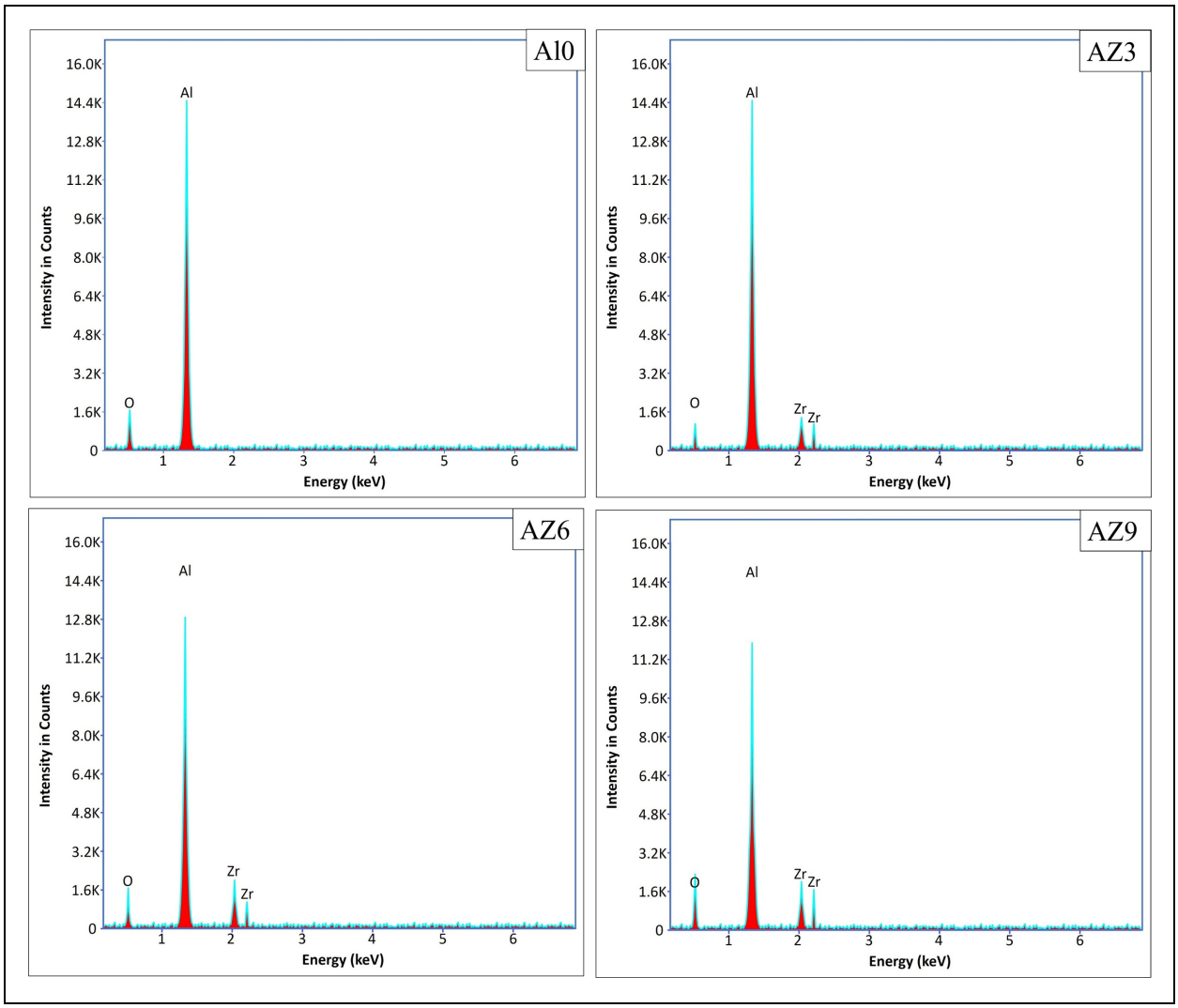


Fig. 6: EDX images for Al/ZrO_2 composites

From the EDX spectra (Fig. 6), it can be verified that ZrO_2 ceramic reinforcement successfully enters the metallic matrix of pure aluminum ($A1_0$) and aluminum matrix composites reinforced with 3% (AZ_3), 6% (AZ_6), and 9% (AZ_9). In the $A1_0$ spectrum, aluminum peak strength (~1.49 keV) prevails while a weaker oxygen peak (~0.52 keV) arises due to natural matrix oxidation. The oxygen peak intensity rises with the addition of ZrO_2 due to the increase in the oxide content. The Zr Lα peak, located at ~2.04 keV, and the Zr Lβ peak at ~2.12 keV are

more pronounced in the analytical spectra of AZ_3, AZ_6, and AZ_9 while intensifying according to the added ZrO_2 content in each sample. The Zr peaks within both AZ_6 and AZ_9 are visible and strong enough to prove ZrO_2 incorporation in the material. The aluminum peak intensity decreases slightly because the spectrum shows evidence of peak displacement from reinforcement-based effects. The results indicate pure elemental composition in the samples because all peaks in the background are clear, and no foreign materials are detected. EDX profiles demonstrate both ZrO_2 particles embedded successfully within the aluminum matrix through spatial mapping of elements that remain uniformly distributed. The results support the successful development of Al/ZrO_2 composites with enhanced ceramic composition.

3.3 Density and Porosity

Fig. 7 shows the theoretical and experimental densities and porosity measurements for $A1_0$, AT_3, AT_6, and AT_9 nanocomposite samples. The experimental density shows a steady reduction compared to the theoretical density when moving from $A1_0$ to AT_9, because these measurements cause the porosity to rise.

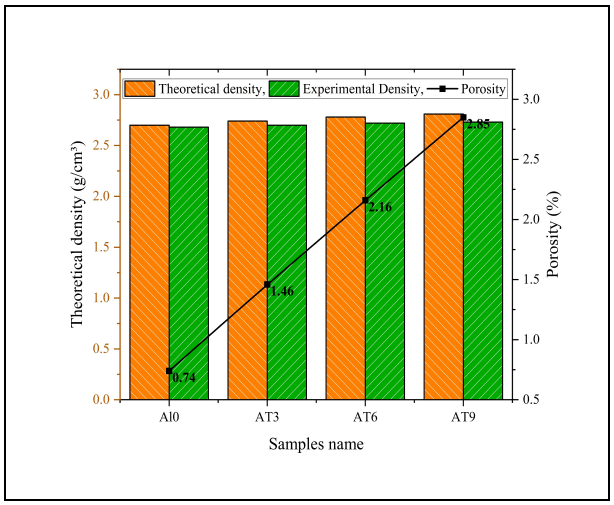


Fig. 7: Density and porosity of Al/TiO_2 composites

The porosity of $A1_0$ stands at 0.74% because it demonstrates minimal variation between theoretical and experimental density standards (Liu *et al.* 2021). AT_9 exhibits the highest porosity value at 2.85% because its high content of nano-reinforcement enhances the chance of particle agglomeration. The densification efficiency of the composite decreases minimally as the reinforcement content increases. AT_3 and AT_6 display intermediate porosity values of 1.46% and 2.16%, respectively. The data presents a developing relationship where material density decreases as the amount of reinforcement material increases.

Fig. 8 shows the theoretical density, experimental density, and porosity among the four nano-composite samples named $A1_0$, AZ_3, AZ_6, and AZ_9 composite samples. Higher reinforcement ratios in the samples starting from $A1_0$ to AZ_9 cause experimental density to separate more than the theoretical density, thus increasing overall porosity. The experimental density of A_{10} matches its theoretical counterpart, which results in minimal sample porosity amounting to 0.74%. The porous structure of AZ_9 material reaches its maximum value at 5.26%, possibly because of non-uniform reinforcement distribution (Zhang and Park, 2019). AZ_3 and AZ_6 samples exhibit intermediate porosity values of 2.14% and 3.41%, respectively. The experiment shows that higher reinforcement volume causes increased material porosity, which results in worse compaction performance. Lesser porosity emerges as the theoretical density slightly rises across all samples because of denser reinforcement phases within each specimen. The diagram illustrates that rising nano-reinforcement content leads to reduced densification of the material.

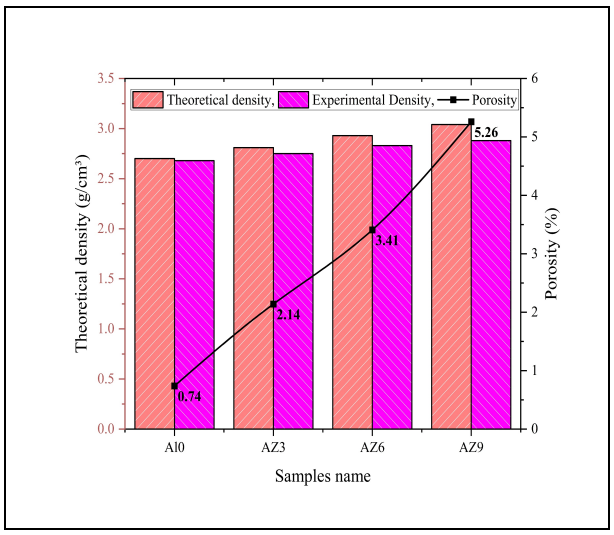


Fig. 8: Density and porosity of Al/ZrO_2 composites

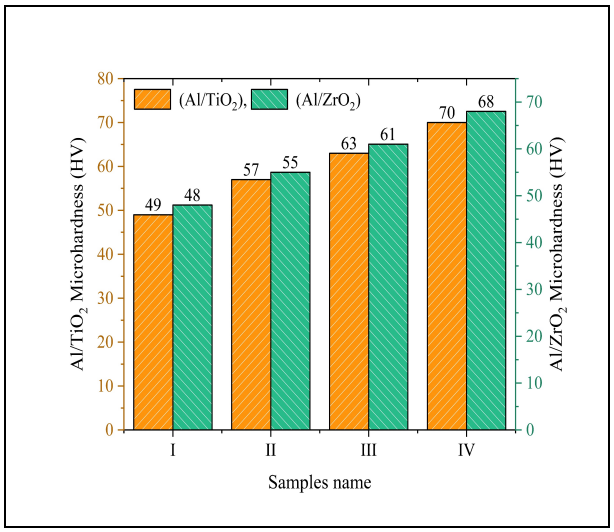


Fig. 9: Microhardness of Al/TiO_2 and Al/ZrO_2 composites

3.4 Microhardness

The microhardness values of the Al/TiO_2 nanocomposites are shown in Fig. 9, demonstrating a consistent improvement of microhardness with increasing TiO_2 content (Sabari *et al.* 2025). The pure aluminum sample $A1_0$ exhibited a microhardness of 49 HV, which is the reference for comparative analysis with nanocomposite samples. The sample AT_3 has incorporated 3 wt.% of TiO_2 nano-ceramics, leading to a noticeable improvement in hardness of 57 HV. The distribution of TiO_2 nanoparticles within the aluminum matrix, which prevents the dislocation movement, accounts for this improvement. Further addition of the nano-reinforcement to 6 wt.% in sample AT_6 has improved microhardness of 63 HV, this demonstrates the optimal particle distribution and robust bonding strength of the reinforcement phase. For 9 wt.% AT_9, the microhardness reaches 70 HV, indicating a 43% increase from that of pure aluminum. This noticeable change verifies the strengthening impact obtained by means of homogeneous ceramic dispersion. Nano-sized TiO_2 particles increase matrix stiffness and cause Orowan looping. Furthermore, significant factors in resisting plastic deformation include the great hardness of TiO_2 itself and strong interfacial bonding. Al/ZrO_2 nanocomposite also shows a progressive enhancement in microhardness with increased ZrO_2 nano content. $A1_0$ sample has recorded a hardness value of 48 HV, which increased with the addition of 3 wt.% ZrO_2 nano-reinforcement of the sample (AZ_3) exhibits the microhardness of 55 HV. For 6 wt.% ZrO_2 reinforcement sample (AZ_6), there is a further increase in the microhardness to 61 HV, indicating the efficient dispersion and interaction between the aluminum matrix and ceramic particles. The improvement of the hardness is the result of multiple strengthening mechanisms, including load transfer to the grain structure, grain refinement, and particle-induced strain hardening. The nano-reinforcement of ZrO_2 has a high modulus and thermal stability, contributing to raising the localized deformation during the indentation. The increasing hardness values indicate the effectiveness of ZrO_2 in resisting plastic flow, which contributes to a reduction in plastic deformation. The improvement seen, which is a bit more than that of the Al/TiO_2 nanocomposite, shows how well ZrO_2 can strengthen the material. This outcome validates the potential of Al/ZrO_2 nanocomposites for demanding engineering applications.

3.5 Thermal Conductivity

The thermal conductivity of the Al/TiO_2 nanocomposite samples decreases as the TiO_2 nano-reinforcement increases. The $A1_0$ sample has the maximum thermal conductivity at room temperature, which is around 3.3 W/m·K. The AT_3 sample has a thermal conductivity of 3.2 W/m·K, which is low compared to the pure aluminum sample $A1_0$, as shown in Fig. 10. It exhibits a thermal conductivity difference decreased by 3% than sample $A1_0$. When the nano-reinforcement in the AT_6 sample is raised to 6 wt.%, the thermal conductivity drops to around 2.9 W/m·K, which is a 12% decline from that of pure aluminum matrix. The AT_9 sample exhibits the lowest conductivity, at roughly 2.7 W/m·K, which is an 18% drop from the $A1_0$ base sample. The heat transfer in the aluminum matrix is reduced by ceramic particles that function as phonon scattering centers. The TiO_2 nanoceramic reinforcement was well dispersed within the aluminum matrix, enhancing the structural stability. The nano-reinforcement acted as a thermal heat prevention to reduce the heat conduction. As the temperature rises from 25 °C to 300 °C, all of the samples show a progressive drop in the thermal conductivity, which was happening to most metals as their lattice vibrations increase. Despite a decrease, AT_9 maintains superior conductivity compared to AT_3 and AT_6 (Wang *et al.* 2018). The analysis indicates that excessive TiO_2 loading adversely affects heat transfer efficiency.

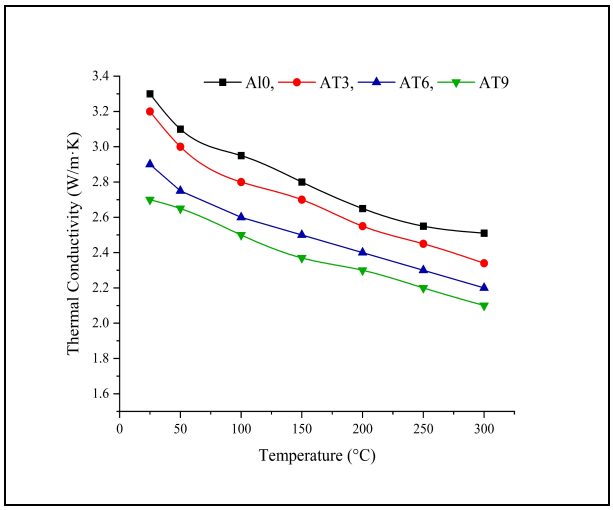


Fig. 10: Thermal conductivity of Al/TiO_2 composites

Fig. 11 shows that the thermal conductivity of Al/ZrO_2 nanocomposites drops as the amount of ZrO_2 reinforcement increases. The sample $A1_0$ has the best thermal conductivity at 30 °C, with a value of around 3.3 W/m·K. The sample AZ_3 has a value of 3.1 W/m·K, which is 6% lower than $A1_0$. The sample AZ_6 lowers even further, to approximately 2.85 W/m·K, which is a 13% decline. The AZ_9 sample exhibits the lowest conductivity of 2.6 W/m·K, representing a 21% reduction. At 100 °C, $A1_0$ drops to 2.95 W/m·K. AZ_3, AZ_6, and AZ_9 exhibit values of 2.8, 2.7, and 2.55 W/m·K, which are drops of 5%, 8%, and 13%, respectively. The sample $A1_0$ recorded 2.65 W/m·K at 200 °C, whereas sample AZ_3 shows 2.5 W/m·K with a 5% decline, and the sample AZ_6 has a thermal conductivity of 2.25 W/m·K, which is 9% lower, and AZ_9 reduces even further to 2.06 W/m·K, which is a 8% drop. The general tendency shows that adding ZrO_2 nano-reinforcement lowers the thermal conductivity.

This is because ZrO_2 has poor thermal conductivity, and phonon scattering increases at the interface between the aluminum matrix and the ceramic particles. Such reductions become more noticeable at higher temperatures since the scattering becomes stronger and the heat conduction channels grow weaker.

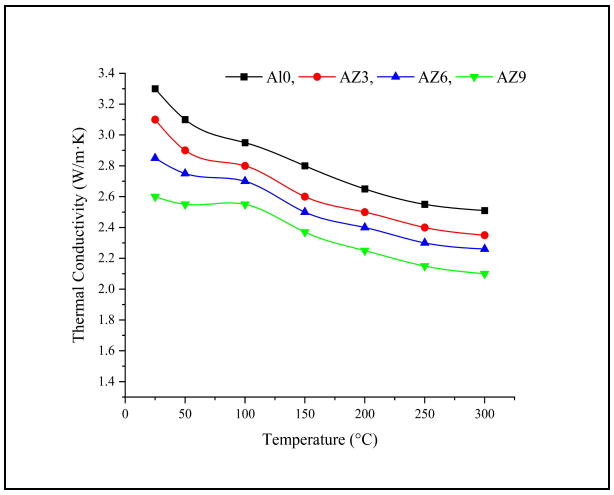


Fig. 11: Thermal conductivity of Al/ZrO_2 composites

In summary, the AT_9 sample has a thermal conductivity of around 2.1 W/m·K at 300 °C, which was 16% lower than the basic sample $A1_0$. The AZ_9 sample, on the other hand, has a reduced thermal conductivity of roughly 2.06 W/m·K at 300 °C, which was a 17.2% drop. This implies that the nanocomposite's thermal conductivity is reduced when both nanoceramics of TiO_2 and ZrO_2 are added individually with an aluminum matrix. But at the same loading level, ZrO_2 nanoceramic has a better effect on lowering heat transmission than TiO_2. The observed trend indicates that ceramic nanoparticles effectively prevent heat from passing through the structure.

4. CONCLUSION

The research focuses on aluminum matrix composites reinforced with nano-ceramic particles, specifically Al/TiO_2 and Al/ZrO_2 nanocomposites. These were fabricated using powder metallurgy techniques at a temperature of 550 °C in a tubular furnace, using TiO_2 and ZrO_2 nano-ceramic particles. The assessment of experimental results and their analyses yielded the following key findings:

- The EDX study shows that the TiO_2 and ZrO_2 nanoparticles were successfully added to the aluminum matrix. A steady increase in the peaks of oxygen and the corresponding ceramic element shows that the dispersion and interaction with the matrix are working well. The steady decrease in the intensity of the aluminum peak shows that there is reinforcement in the matrix and that it has an effect. Both Al/TiO_2 and Al/ZrO_2 nanocomposites have a uniform distribution of elements, which demonstrates that they were built well.

- The density test results indicated that densification decreased when the ceramic content of the samples increased. Experimental data showed pure aluminum specimens reached almost theoretical density amounts (99.26%), yet the Al-9% TiO_2 nanocomposite series contained 2.85% porosity, and the Al-9% ZrO_2 series had 5.26% porosity. The porosity levels of ZrO_2 exceeded those of TiO_2 composites at the same loading since ZrO_2 has a higher density mismatch with the aluminum matrix.

- Microhardness experiments on Al/TiO_2 and Al/ZrO_2 nanocomposites indicate that ceramic nanoparticles strengthen the aluminum matrix. Because load is carried well, particles are spread out, and connections between components are strong, both composites get tougher as reinforcement increases. TiO_2 makes objects tougher due to Orowan strengthening and high intrinsic hardness. ZrO_2 stands out for its thermal stability and high modulus, making it more resistant to plastic deformation. With equal reinforcing, the Al/TiO_2 nanocomposite has slightly greater microhardness than Al/ZrO_2. These findings demonstrate that both nanocomposites are suitable for challenging structural and load-bearing applications.

- Ceramic reinforcement greatly affects heat transfer capacity in Al/TiO_2 and Al/ZrO_2 nanocomposites, as shown by their thermal conductivity behaviour. The decrease in thermal conductivity with increasing reinforcement is due to the nano-ceramic particles' phonon scattering effect, which blocks heat carrier movement in the aluminum matrix. Al/TiO_2 composites have a steady conductivity fall, peaking at 16% for 9 wt.% reinforcement, whereas Al/ZrO_2 composites exhibit a faster reduction, reaching 17.2% at the same level. These findings show the trade-off between mechanical enhancement and thermal conductivity in nanocomposites, guiding reinforcement level selection for application-specific thermal needs.

ACKNOWLEDGEMENTS

The authors are thankful to the Saveetha School of Engineering, Saveetha Institute of Medical and Technical Sciences for infrastructure, lab facilities, and constant support for this Research work.

FUNDING

This research received no specific grant from any funding agency in the public, commercial, or not-for-profit sectors.

CONFLICTS OF INTEREST

The authors declare that there is no conflict of interest.

COPYRIGHT

This article is an open-access article distributed under the terms and conditions of the Creative Commons Attribution (CC BY) license (http://creativecommons.org/licenses/by/4.0/).

REFERENCES

Arif, S., Alam, M. T., Ansari, A. H., Siddiqui, M. A., and Mohsin, M., Study of mechanical and tribological behaviour of Al/SiC/ZrO_2 hybrid composites fabricated through powder metallurgy technique, *Mater. Res. Express.,* 4(7), 76511(2017). https://doi.org/10.1088/2053-1591/aa7b5f

Boehlert, C. J., Hernández-Escobar, D., Ruiz-Palenzuela, B., Sabirov, I., Cornide, J., and Ruiz-Navas, E. M., The effect of microstructure and strain rate on the 25 °C and 700 °C compression deformation behavior of powder metallurgy processed Ti-45Al-2Nb-2Mn (at.%)-0.8 TiB2 (vol%) alloy, *Mater. Charact.,* 172, 110856(2021). https://doi.org/10.1016/j.matchar.2020.110856

Joshua, K. J., Vijay, S. J. and Selvaraj, D. P., Effect of nano TiO_2 particles on microhardness and microstructural behavior of AA7068 metal matrix composites, *Ceram. Int.,* 44(17), 20774–20781(2018). https://doi.org/10.1016/j.ceramint.2018.08.077

Juliyana, S. J., Prakash, J. U., Salunkhe, S., Hussein, H. M. A. and Gawade, S. R., Mechanical Characterization and Microstructural Analysis of Hybrid Composites (LM5/ZrO_2/Gr), *Cryst.,* 12(9), 1207(2022). https://doi.org/10.3390/cryst12091207

Kennedy, E., Sachin, B. S., Ramachandra, M., Niranjan, C. A., Sriraman, N., Jain, V. K. S., and Sathiya Narayanan, N., Effect of ZrO_2 nano-particles on mechanical and corrosion behaviour of Al2024 alloy, *Mater. Today Proc.,* 39, 1710–1713(2021). https://doi.org/10.1016/j.matpr.2020.06.194

Khan, A., Abdelrazeq, M. W., Mattli, M. R., Yusuf, M. M., Alashraf, A., Matli, P. R. and Shakoor, R. A., Structural and mechanical properties of Al-SiC-ZrO_2 nanocomposites fabricated by microwave sintering technique, *Cryst.,* 10(10), 904(2020). https://doi.org/10.3390/cryst10100904

Kishore M. T., Kumar, P., and Jain, P., Effects of graphene content on the wear properties of aluminum matrix composites prepared by powder metallurgy route, *Mater. Today Proc.,* (2023). https://doi.org/10.1016/j.matpr.2023.07.074

Kumar, N. and Irfan, G., A review on tribological behaviour and mechanical properties of Al/ZrO_2 metal matrix nano composites, *Mater. Today Proc.,* 38, 2649–2657(2021). https://doi.org/10.1016/j.matpr.2020.08.240

Liu, Y., Yao, M. and Yao, X., Enhancement of energy storage density achieved in Bi-modified SrTiO3 thin films by introducing a TiO_2 layer, *J. Alloys Compd.,* 882, 160668(2021). https://doi.org/10.1016/j.jallcom.2021.160668

Luqman, M., Ali, Y., Zaghloul, M. M. Y., Sheikh, F. A., Chan, V. and Abdal-hay, A., Grain refinement mechanism and its effect on mechanical properties and biodegradation behaviors of Zn alloys – A review, *J. Mater. Res. Technol.,* 24, 7338–7365(2023). https://doi.org/10.1016/j.jmrt.2023.04.219

Madhusudhana, S., Prakash, J. N. and Manjunath, L. H., Study on preparation and mechanical characterization of aluminum-albite composites using powder metallurgy technique, *Mater. Today Proc.,* 54, 390–394(2022). https://doi.org/10.1016/j.matpr.2021.09.456

Manohar, G., Maity, S. R. and Pandey, K. M., Effect of Sintering Temperatures on Mechanical Properties of AA7075/B4C/Graphite Hybrid Composite Fabricated by Powder Metallurgy Techniques, *Recent Adv. Mech. Eng.,* 343–350(2021). https://doi.org/10.1007/978-981-15-7711-6_35

Najjar, I. R. and Elmahdy, M., Study of mechanical properties and wear resistance of nanostructured Al 1100/TiO_2 nanocomposite processed by accumulative roll bonding, *J. Compos. Mater.,* 56(17), 2727–2738(2022). https://doi.org/10.1177/00219983221103636

Najjar, I., Sadoun, A., Alam, M. N. and Fathy, A., Prediction of wear rates of Al-TiO_2 nanocomposites using artificial neural network modified with particle swarm optimization algorithm, *Mater. Today Commun.,* 35, 105743(2023). https://doi.org/10.1016/j.mtcomm.2023.105743

Nayak, K. C., Rane, K. K., Date, P. P., and Srivatsan, T. S., Synthesis of an Aluminum Alloy Metal Matrix Composite Using Powder Metallurgy: Role of Sintering Parameters, *Appl. Sci.,* 12(17), 8843(2022). https://doi.org/10.3390/app12178843

Panwar, N., Chauhan, A., Singh Pali, H. and Dutt Sharma, M., Fabrication of Aluminum 6061 Red-mud Composite using Stir Casting and Micro Structure Observation, *Mater. Today Proc.,* 21, 2014–2023(2020). https://doi.org/10.1016/j.matpr.2020.01.318

Randis, R., Darmadi, D. B., Gapsari, F., Sonief, A. A., Akpan, E. D., and Ebenso, E. E., The potential of nanocomposite-based coatings for corrosion protection of metals: A review, *J. Mol. Liq.,* 390, 123067(2023). https://doi.org/10.1016/j.molliq.2023.123067

Sabari, K., Muniappan, A., Deepanraj, B. and Mohamed, M. J. S., Enhancing Mechanical Performance of Friction Stir Welded AZ31 Magnesium Alloy with Nano-TiC Reinforcements Using Grey Relational Analysis, *Int. J. Precis. Eng. Manuf.,* 26, 27-41(2025). https://doi.org/10.1007/s12541-024-01096-3

Sabari, K., Muniappan, A., Deepanraj, B., and Yuvaperiyasamy, M., Exploring the Effect of TiO_2 Nanoparticles on the Microstructural Dynamics and Mechanical Attributes of Dissimilar FSW Joints Between AA7071 and AZ31, *Trans. Indian Inst. Met.,* 78(3), (2025). https://doi.org/10.1007/s12666-024-03535-1

Samal, P., Vundavilli, P. R., Meher, A., and Mahapatra, M. M., Recent progress in aluminum metal matrix composites: A review on processing, mechanical and wear properties, *J. Manuf. Processes.,* 59, 131–152(2020). https://doi.org/10.1016/j.jmapro.2020.09.010

Sezgin, A., Čtvrtlík, R., Václavek, L., Tomáštík, J., Nožka, L., Menşur, E., and Türküz, S., Optical, structural and mechanical properties of TiO_2 and TiO_2-ZrO_2 thin films deposited on glass using magnetron sputtering, *Mater. Today Commun.,* 35, 106334(2023). https://doi.org/10.1016/j.mtcomm.2023.106334

Singh, H., Bahri, H. and Singh, K. K., Experimental Analysis of Wear and Mechanical Characteristics of Aluminium Matrix Composite Fabricated Through Powder Metallurgy, *Comput. Exp. Methods Mech. Eng.,* 115–129(2021). https://doi.org/10.1007/978-981-16-2857-3_14

Song, X., Ding, Y., Zhang, J., Jiang, C., Liu, Z., Lin, C., Zheng, W. and Zeng, Y., Thermophysical and mechanical properties of cubic, tetragonal and monoclinic ZrO_2, *J. Mater. Res. Technol.,* 23, 648–655(2023). https://doi.org/10.1016/j.jmrt.2023.01.040

Sunil, K. K., Kalos, P. S., Akhtar, M. N., Shaik, S., Sundara, V., Fayaz, H., Khan, S. A., and Asif, M., Experimental and theoretical analysis of exhaust manifold by uncoated and coated ceramics (Al_2O_3, TiO_2 and ZrO_2), *Case Stud. Therm. Eng.,* 50, 103465(2023). https://doi.org/10.1016/j.csite.2023.103465

Surakasi, R., Prasad, A. R., Pattnaik, B., Rao, M. V., Puthilibai, G., Vibhakar, C., and Rajkumar, S., Mechanical behavior of nanoceramic-reinforced aluminum matrix composites, *Mater. Today Proc.,* 59, 1452–1456(2022). https://doi.org/10.1016/j.matpr.2022.01.085

Wang, Q., Guo, L., Yan, Z. and Ye, F., Phase Composition, Thermal Conductivity, and Toughness of TiO_2-Doped, Er2O3-Stabilized ZrO_2 for Thermal Barrier Coating Applications, *Coat.,* 8(7), 253(2018). https://doi.org/10.3390/coatings8070253

Xavier, J. R., Electrochemical and dynamic mechanical properties of polyurethane nanocomposite reinforced with functionalized TiO_2–ZrO_2 nanoparticles in automobile industry, *Appl. Nanosci.,* 12(5), 1763–1778(2022). https://doi.org/10.1007/s13204-022-02393-x

Zhang, A. and Li, Y., Thermal Conductivity of Aluminum Alloys—A Review, *Mater*., 16(8), 2972(2023). https://doi.org/10.3390/ma16082972

Zhang, K. and Park, S. S., Effects of current density on anodizing behavior, micro-structure, and electrical properties of ZrO_2-coated Al foils, *Appl. Surf. Sci.,* 477, 44–49(2019). https://doi.org/10.1016/j.apsusc.2018.01.119